Three-dimensional laser cooling method based on resonant linear coupling

T. Kihara, H. Okamoto,* and Y. Iwashita

Accelerator Laboratory, Institute for Chemical Research, Kyoto University, Gokanoshou, Uji, Kyoto 611-0011, Japan

K. Oide

High Energy Accelerator Research Organization (KEK), Oho, Tsukuba, Ibaraki 305-0801, Japan

G. Lamanna

INFN, Dipartimento di Fisica dell'Universita' di Bari, Via Amedola 173 70126 Bari, Italy

J. Wei

Brookhaven National Laboratory, Upton, New York 11973

A three-dimensional (3D) laser cooling method of fast stored ion beams based on a linear coupling mechanism is explored. We extensively study two approaches proposed in previous publications, i.e., the dispersive coupling scheme and the coupling-cavity scheme, confirming how much one can improve the transverse cooling efficiency. A possible design of a coupling cavity is presented. We employ the tracking code SAD and the molecular dynamics code SOLID to carry out reliable numerical experiments where realistic lattice structures of storage rings and particle Coulomb interactions are taken into account. Through systematic simulations, it is demonstrated that resonant coupling remarkably enhances transverse cooling rates for any initial beams, making it feasible to reach an equilibrium temperature far below the current achievable level. We further emphasize the crucial importance of avoiding the Mathieu instability. We also discuss the minimum cooling power required for beam crystallization as well as on an interpretation of past experimental results in the TSR and ASTRID storage rings. [S1063-651X(99)04803-5]

PACS number(s): 41.75.−i, 29.20.Dh, 61.50.−f, 52.25.Wz

I. INTRODUCTION

During the past several decades, various cooling techniques of charged hadron beams have been invented and experimentally tested—stochastic cooling [1], electron cooling [2], and Doppler laser cooling [3]. By increasing the phase-space density of the beam, these techniques have played crucial roles for rare particle (antiproton and radiative particles) collection, for beam stacking, for emittance preservation, and for luminosity improvements. To our current knowledge, Doppler laser cooling is the most promising technique in achieving the highest possible phase-space density of ion beams. The limiting temperature attainable with this cooling method is below mK, sufficient to realize the theoretically predicted phase transition of fast stored beams [4]. In fact, ion crystallization has been experimentally observed in rf traps as well as static traps using laser cooling. For cooling of fast stored beams, presently two storage rings, i.e. the TSR ring in Germany [5] and the ASTRID ring in Denmark [6], are equipped with laser coolers, where beam temperatures much lower than those ever recorded with other techniques have been obtained in the *longitudinal* direction of beam motion. The success achieved by the TSR and ASTRID groups has now allowed us to reasonably anticipate that one may be able to produce crystalline beams in the near future.

In contrast with the experimental success in reducing the longitudinal beam temperature to an ultracold range, laser cooling in the transverse directions has been much less effective. Although the natural Coulomb interaction between individual particles can be a source of heat exchange, its rate is low. In past experiments [7], the transverse temperature appeared to saturate far above the final longitudinal temperature. As this difficulty has not been overcome in the last decade, in spite of continuous experimental effort, it is now thought that one may need to develop another approach in order to extend the powerful laser cooling force to the transverse degrees of freedom.

In previous papers [8,9], Okamoto, Sessler, and Möhl first proposed the idea of using artificial dynamical coupling to indirectly provide a strong transverse dissipative force. The coupling source theoretically considered was the linear potential induced either by a special *coupling cavity* operating in the TM_{210} mode [8] or by *momentum dispersion* in a regular rf cavity [9]. It was proved that the transverse cooling rates can be considerably enhanced under the resonance conditions

$$\nu_x - \nu_s \approx k, \quad \nu_x - \nu_y \approx l \quad (k,l = \text{integer}), \qquad (1)$$

where ν_x and ν_y are the horizontal and vertical betatron tunes, and ν_s is the synchrotron tune. A significant feature of these proposed schemes is their simplicity; they are well within the scope of existing technology. For instance, in the dispersive coupling scheme we only need to install an ordinary accelerating cavity at a location where the dispersion is finite. Clearly, it is possible to test the validity of the basic

---

*Present address: Department of Quantum Matter, Graduate School of Advanced Sciences of Matter, Hiroshima University, 1-3-1 Kagamiyama, Higashi-Hiroshima 739-8526, Japan.

idea in the TSR and/or ASTRID ring only by making minor modifications to the lattice parameters. In fact, a very recent experiment [10] has demonstrated the effectiveness of the resonant coupling method.

In Sec. II, we first evaluate the efficiency of various resonant coupling schemes described in Refs. [8] and [9]. After a brief review, in Sec. III we present a possible design of the coupling rf cavity. In Sec. IV, single-particle simulations, incorporating the actual lattice parameters of several existing cooler rings, are performed with the tracking code SAD (Strategic Accelerator Design) [11] to investigate the cooling characteristics in the high-temperature regime systematically. In Sec. V, the molecular dynamics (MD) approach is further employed to incorporate the effect of Coulomb interactions which dominates the beam at low temperature. Finally in Sec. VI, we attempt to answer questions such as the

following: ''What is the lowest transverse temperature achievable with the coupling method ?'' ''Why is the imbalance of equilibrium beam temperatures so large between the longitudinal and transverse directions in TSR and ASTRID?'' ''How great a cooling rate is necessary in an ideal situation to reach the lowest possible temperature ?'' ''Is laser cooling of fast stored beam really only longitudinally powerful?''

II. THREE-DIMENSIONAL LASER COOLING SCHEMES

A. Dispersive coupling in a rf cavity

Consider an ordinary storage ring consisting of dipole magnets, quadrupole magnets, and a regular rf cavity. The single-particle Hamiltonian governing this dynamical system can be written, in smooth approximation, as [9]

$$H_1 = \frac{1}{2}(p_x^2 + \nu_x^2 x^2) + \frac{1}{2}(p_y^2 + \nu_y^2 y^2) - \frac{\eta W^2}{2} + \Gamma_q y \left(x - \frac{D_x}{R} W \right) \delta_p(\theta - \theta_q) - \frac{h_b q V_b}{p_0 \beta_0 c} \cos \left[\psi - \frac{1}{R} \left(D_x p_x - \frac{dD_x}{d\theta} x \right) \right] \delta_p(\theta - \theta_b),$$

(2)

where the canonical variables $(x, p_x, y, p_y, \psi, W)$ have been scaled to be dimensionless [12], $\delta_p(z)$ is the periodic δ function with a periodicity of 2π, and the independent variable θ is defined as $\theta = s/R$, with R and s being, respectively, the average radius of the ring and path length along the design orbit. Other parameters appearing in Eq. (2) are η, the phase slip factor; p_0, the design kinetic momentum; q, the charge state of stored ions, h_b, the harmonic number of the rf system; V_b, the voltage of the rf system; β_0, the Lorentz factor; D_x, the horizontal dispersion function; Γ_q, the skew coupling factor; c, the speed of light; θ_b, the longitudinal coordinate at the rf cavity; and θ_q, the longitudinal coordinate at the skew quadrupole. The skew quadrupole field, corresponding to the fourth term on the right hand side of Eq. (2), is needed to couple the vertical motion to the horizontal motion. When the axial length of the skew magnet is L_q, the coupling factor Γ_q can be defined by

$$\frac{\Gamma_q}{R} = \frac{L_q}{B\rho} \left(\frac{\partial B}{\partial y} \right),$$

(3)

where B is the magnetic field, and $B\rho$ is the magnetic rigidity. Instead of a skew quadrupole magnet, a solenoid can, of course, also be used for horizontal-vertical coupling [8].

Specifically, the rf potential represented by the last term in Eq. (2) yields a synchrobetatron coupling, provided that either the function D_x or the θ derivative of D_x is nonzero at the location of the rf cavity. Although the rf coupling involves not only linear but also nonlinear components, the linear contribution is of primary importance. Through this coupling potential, the longitudinal dissipative force due to laser photons can be effectively extended to the transverse degrees of freedom under the condition of Eq. (1). Needless to say, the mixing of the three harmonic motions, i.e., synchrotron motion and betatron motion, is always present un-

less we turn off the coupling fields. However, when the operating point of a storage ring is far away from the coupling resonance, no dramatic cooling effect will take place in the transverse directions.

B. Coupling-cavity scheme

An alternate way to artificially generate a strong synchrobetatron coupling is to use a dedicated coupling cavity. From the above discussion, it is mathematically evident that the key item is the second-order potential proportional to the product $x\psi$ (or $y\psi$). Such a term can be created by means of a special *coupling cavity* excited in a TM_{210} mode [8]. Assuming a simple rectangular pillbox cavity of width $2a$ and height $2b$, the vector potential for this mode is given by

$$\mathbf{A}_c = \left(0, 0, \frac{V_c}{\omega_c} \sin \left(\frac{\pi x}{a} \right) \cos \left(\frac{\pi y}{2b} \right) \sin(\omega_c t + \phi_c) \right),$$

(4)

where V_c and ω_c denote the voltage and angular frequency of the coupling rf field, and ϕ_c is the initial phase. Equation (4) indicates that, in the paraxial approximation, the longitudinal electric field of the cavity is linearly dependent on the horizontal coordinate x and, thus, can be a source of linear synchrobetatron coupling. Neglecting the dispersive effects for the sake of simplicity, the approximate Hamiltonian for the coupling-cavity scheme takes the form [13]

$$H_2 = \frac{1}{2}(p_x^2 + \nu_x^2 x^2) + \frac{1}{2}(p_y^2 + \nu_y^2 y^2) - \frac{\eta W^2}{2}$$

$$- \frac{h_b q V_b}{p_0 \beta_0 c} \cos \psi \delta_p(\theta - \theta_b) + \Gamma_q x y \delta_p(\theta - \theta_q)$$

$$- \frac{2\pi h_b \Gamma_c}{h_c} x \sin \left(\frac{h_c}{h_b} \psi \right) \delta_p(\theta - \theta_c),$$

(5)

where h_c is the harmonic number of the coupling cavity sitting at $\theta = \theta_c$, and Γ_c is the coupling strength fully dependent on the cavity design. Obviously, the lowest order term of the coupling-cavity potential is proportional to $x\psi$ as required.

The coupling-cavity scheme has two unique features. First, it is straightforward to develop a direct coupling between longitudinal and vertical direction by means of a *vertical* coupling cavity, i.e., with the coupling cavity being rotated by 90° around the beam line. Second, the transverse cooling rates can be further enhanced from those of the rf dispersive coupling method discussed in Sec. II A. The main reason for this is that, in the coupling-cavity scheme, we always have to turn on a regular cavity as well in order to satisfy the resonance condition [14]. This implies that the rf dispersive coupling is also activated as long as the dispersion is finite at the location of the regular rf cavity—we have the couplings originating from two separate sources.

C. Coupling resonance width

We now estimate the sensitivity of transverse cooling efficiency to the resonance condition. Consider only the longitudinal-horizontal dispersive coupling for brevity. The cooling rate per revolution can be derived as (see the Appendix)

$$\Lambda_x = \frac{(1-g)\Lambda}{2} \quad \text{for the horizontal motion,} \quad (6a)$$

$$\Lambda_s = \frac{(1+g)\Lambda}{2} \quad \text{for the longitudinal motion,} \quad (6b)$$

where we have assumed a smooth longitudinal cooling force having a friction coefficient Λ,

$$g = \frac{|\cos(2\pi\nu_x) - \cos(2\pi\nu_s)|}{\sqrt{[\cos(2\pi\nu_x) - \cos(2\pi\nu_s)]^2 + \xi^2 \sin(2\pi\nu_x)\sin(2\pi\nu_s)}},$$
$$(7)$$

and the coupling constant ξ is defined by

$$\xi^2 = \frac{2\pi h_b q V_b}{p_0 \beta_0 c}\left(\frac{D_b}{R}\right)^2, \quad (8)$$

where D_b is the dispersion at the location of the rf bunching cavity. In this analysis, terms of order higher than ξ^2 and Λ are neglected. Note that the sum of the horizontal and longitudinal rates in Eqs. (6) is equal to a constant, Λ, which is a result of energy conservation.

Equations (6) and (7) indicate that the horizontal cooling rate grows as the synchrotron tune ν_s approaches the fractional part of the betatron tune ν_x. The two cooling rates become the same when $\cos(2\pi\nu_x) = \cos(2\pi\nu_s)$. The full width half maximum of this resonance peak with respect to ν_s can be obtained as

$$\delta\nu_s \approx \frac{\xi}{\sqrt{3}\,\pi}. \quad (9)$$

III. A POSSIBLE DESIGN OF THE COUPLING CAVITY

Before proceeding to numerical simulations, in this section we present a possible design of the coupling cavity. Our first task is to determine the operating rf frequency. In order to reduce unnecessary nonlinear effects during the cooling process, the bucket length of the coupling-cavity field needs to be shorter than or equal to that of the bunching rf field, namely, $h_c \leq h_b$. For simplicity, we assume $h_c = h_b$ in the following discussion [15].

The rf harmonic numbers used for bunched-beam laser cooling in TSR and ASTRID are moderate—typically less than 30. For the application of resonant coupling schemes, however, h_b needs to be much greater to ensure a relatively high synchrotron tune with a low rf voltage. Here we specify V_b to be of the order of 100 V or less based on the experience of past cooling experiments in ASTRID [16]. On the other hand, the synchrotron tune ν_s has to be sufficiently large to provide adequate clearance from the transverse integer stopbands [under the condition of Eq. (1)]. To meet these two contradictory requirements, a beam of lower kinetic energy is preferred. While the minimum resonance stopband width depends on the condition of machine imperfection, we consider ν_s up to 0.1 to reserve adequate distance from the stopbands in this paper.

For the pill-box geometry considered in Eq. (4), the rf frequency f_c $(= \omega_c/2\pi)$ satisfies

$$\frac{1}{a^2} + \frac{1}{(2b)^2} = \left(\frac{2f_c}{c}\right)^2. \quad (10)$$

Obviously, the cavity dimension becomes excessively large unless the frequency is chosen to be sufficiently high. In fact,
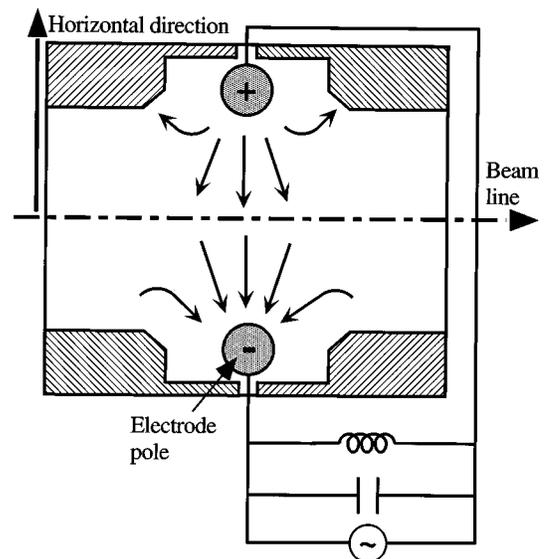
FIG. 1. Conceptual layout of a coupling cavity. rf power is supplied directly to the two electrodes by an external circuit. To generate a dipolelike electric field near the beam line, rf voltages of opposite signs are applied to the electrodes.
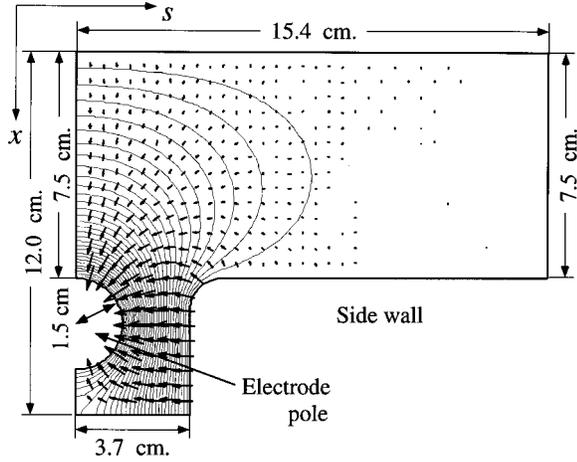
FIG. 2. A possible coupling-cavity design. One-quarter of the cavity has been drawn. The solid curves inside the cavity represent the equipotential lines obtained from the POISSON code, and the small arrows show the directions of the electric field.

FIG. 3. The effective fields of the coupling cavity defined by Eqs. (11). The interelectrode voltage has been set at 2 V.

even for a frequency in the range of several hundred MHz, the cavity size is still of the order of 1 m. Assuming ^{24}Mg$^+$ ions stored in the ASTRID ring at a total energy of 100 keV, the harmonic number will then exceed several thousand corresponding to the rf bucket length of less than 1 cm. Therefore, from a practical point of view, here we devise a special lumped circuit instead of a simple rectangular resonator, yielding a much lower design frequency.

Designing a proper lumped circuit is actually straightforward. Since the axial electric field of a coupling cavity is proportional to $x \cos(\omega_c t + \phi_c)$ near the beam line, we design a cavity with a geometry to produce a dipolelike field. Consider a simple structure such as depicted in Fig. 1, i.e., a rectangular box with two electrodes standing across the beam line. The longitudinal dimension of the cavity is approximately equal to $2\beta_0 c / f_c$. To excite the coupling field, the electrode poles are connected to an external circuit feeding rf power at the design frequency. The frequency is simply determined by the external electronics devices.

To give an example of the coupling-cavity design, we again consider the ASTRID ring storing a 100-keV ^{24}Mg$^+$ beam. We choose $h_c = h_b = 260$, which is ten times larger than that of the usual ASTRID operation. The corresponding rf frequency is 5.78 MHz. At this harmonic number, the rf voltage required for $\nu_s = 0.1$ is only about 37 V. In order to analyze the electromagnetic field distribution of the coupling cavity precisely, it is indeed necessary to employ a three-dimensional (3D) Maxwell equation solver. On the other hand, since the cavity dimension is much smaller than the rf wavelength, we can approximately treat the case as a static problem, thus using the POISSON code [17] for a quick evalu-

ation of the coupling field. Figure 2 displays a coupling-cavity design, assuming that the structure is spatially homogeneous in the vertical direction. In deciding the geometrical parameters, we particularly demand the following points: (a) the cavity size is modest, (b) the coupling coefficient Γ_c is as large as possible, and (c) the field disturbance by the end plates and the beam holes is negligible.
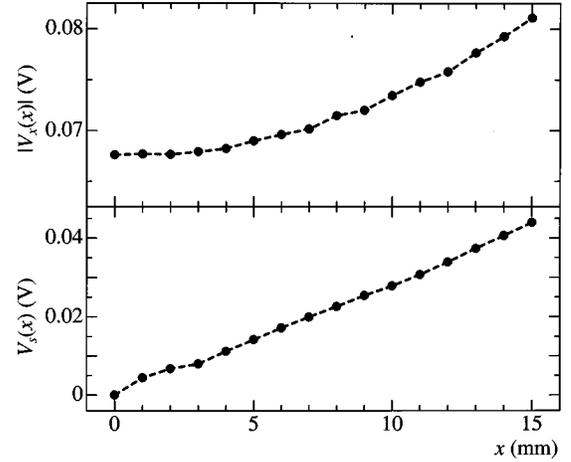
The use of the field data in Fig. 2 enables us to estimate how much coupling can be generated at a specific amount of supplied power. To evaluate the net effect of the cavity field on the particle orbits, we introduce the x-dependent functions

$$\overline{V_x} = -\int_{-L_c/2}^{L_c/2} \frac{\partial V}{\partial x} \cos\left(h_c \frac{s}{R}\right) ds, \tag{11a}$$

$$\overline{V_s} = -\int_{-L_c/2}^{L_c/2} \frac{\partial V}{\partial s} \sin\left(h_c \frac{s}{R}\right) ds, \tag{11b}$$

where V is the scalar potential calculated from POISSON, L_c is the axial length of the cavity, and the origin of the longitudinal coordinate is located at the center of the cavity. In Fig. 3, these integral-field functions are plotted for the geometry of Fig. 2, where the electrode voltage is assumed to be ± 1 V. Apparently, the longitudinal field component of the coupling cavity is linearly dependent on the horizontal coordinate x in the vicinity of the beam line, which is consistent with Eq. (4). Expanding Eqs. (11) into power series as

$$\overline{V_j} = V_c\left[\zeta_{j0} + \zeta_{j1}\left(\frac{x}{d}\right) + \zeta_{j2}\left(\frac{x}{d}\right)^2 + \zeta_{j3}\left(\frac{x}{d}\right)^3 + \cdots\right]$$

$$(j = x \text{ or } s), \tag{12}$$

where d is the scaling constant, chosen here to be 1 cm, the

TABLE I. The expansion coefficients in Eq. (12), where the cavity geometry exhibited in Fig. 2 has been assumed.

	ζ_{j0}	ζ_{j1}	ζ_{j2}	ζ_{j3}
$V_x(j=x)$	-6.7606×10^{-2}	6.7108×10^{-4}	-6.4157×10^{-3}	-4.2928×10^{-6}
$V_s(j=s)$	5.7765×10^{-4}	2.8741×10^{-2}	-4.1517×10^{-3}	2.8549×10^{-3}

expansion coefficients are found as in Table I, showing that ζ_{s1} is dominant. (The constant offset ζ_{x0} has no impact on the beam dynamics.) In the present design, the distance between the electrodes has been chosen to be rather large to eliminate possible aperture limitation. If the interelectrode distance is shortened, the value of ζ_{s1} can be increased accordingly.

IV. SAD TRACKING RESULTS

In general, ion beams circulating in storage rings are quite hot and thin in all three degrees of freedom, which implies that intraparticle collisions through the Coulomb fields are initially negligible. For studies in this high-temperature regime, the MD approach is often computationally too time consuming. Instead, we use the tracking code SAD [11] to explore the hot beam behavior systematically. In order to incorporate the effect of coupling cavities into SAD, here we employ the effective fields in Eq. (12) under the thin lens approximation. Furthermore, for the laser-cooling process, we have added another subroutine where a longitudinal dissipative force is applied to simulation particles. As shown systematically in Fig. 4, we first preset the width Δw of the laser-cooling band to be much smaller than the rf bucket height. (Δw is associated with the limiting temperature reachable in the simulation.) The cooling band sits near the top of the bucket at the beginning, and is then scanned down to the $\delta p/p = 0$ axis at a certain speed. During this scanning process, ions which happen to be inside the band when traversing the cooling section lose energy in the amount of Δw. In this way, the beam is gradually compressed into a tiny region around the origin unless the scanning speed of the cooling band is too fast compared to the synchrotron oscillation cycle.

As an example, we first study with computer simulation the typical operating condition of ASTRID, where $\nu_x = 2.29$ and $\nu_y = 2.73$ (see Table II). The stored particles are 100-keV $^{24}Mg^+$ ions, as have been actually used in recent cooling experiments in ASTRID. The harmonic number of the accelerating cavity is 26. The rf voltage is linearly increased from 0 to 10 V within the first 10^3 turns in order to capture the initial continuous beam adiabatically into the rf buckets. After this beam capturing procedure, the laser cooling band is scanned in the subsequent 10^5 turns. We then obtain Fig. 5(a), in which no transverse cooling is visible. In contrast, we now increase the quadrupole strengths so that $\nu_x = 3.11$ and $\nu_y = 3.09$. A pure skew quadrupole magnet with Γ_q

TABLE II. The main ASTRID parameters in the normal operating mode.

Quantity	Value
Ring circumference $2\pi R$	40 m
Betatron tunes (ν_x, ν_y)	(2.29, 2.73)
Dipole bending radius	6.366 m
Lattice superperiodicity N_l	4
Transition energy γ_T	4.58
rf harmonic number	26

=0.48 is also added to couple the horizontal and vertical motions. We adjust the synchrotron tune to 0.1, increasing the harmonic number to 260. The SAD result based on this resonant situation is given in Fig. 5(b). The effectiveness of the coupling scheme is evident.

To evaluate the dependence of the cooling efficiency on the resonance condition, we perform a series of simulations, varying the synchrotron tune over a wide range. The lattice condition is taken to be exactly the same as that of Fig. 5(b). As indicated by the solid curves in Fig. 6, the final transverse emittances rapidly increase in the region $\nu_s \lesssim 0.05$, due to the reduction of cooling efficiency. The approximate cooling rates evaluated from SAD simulations are also displayed in Fig. 7, where significant enhancement of transverse dissipation around the coupling resonance has been verified. The resonance width estimated by Eq. (9) is about 0.033, which agrees fairly well with this tracking result.
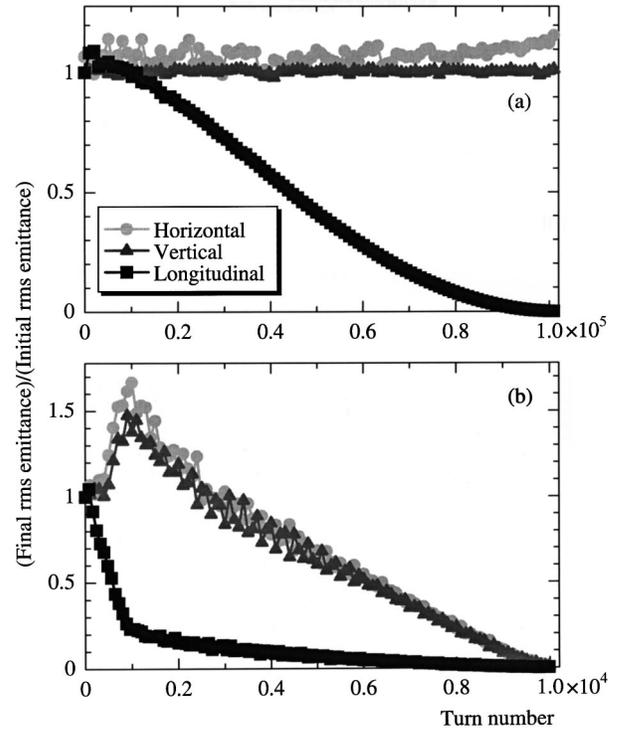
FIG. 5. SAD simulation results. The time evolutions of root-mean-squared (rms) beam emittances are plotted. Case (a) corresponds to the ordinary operating mode of ASTRID, while the lattice parameters have been modified in case (b) such that the resonance conditions in Eq. (1) are roughly satisfied. Notice that the cooling process can be shortened in case (b) because of the high synchrotron tune.

FIG. 4. Longitudinal laser-cooling model employed in the SAD code. $\delta p/p$ is the momentum deviation from the design value.
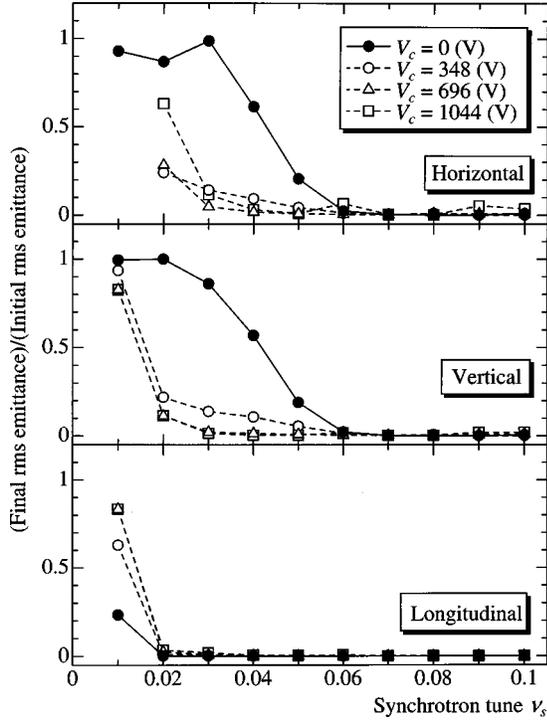
FIG. 6. The ratio of final to initial rms emittances vs operating synchrotron tune. The solid curves represent the case where only dispersive rf coupling is present. We have also tried three different cases of the coupling-cavity scheme (the dotted curves); i.e., $V_c =$ 348 V (open circles), $V_c = 696$ V (triangles), and $V_c = 1044$ V (squares).

In the bunched-beam operation, the coupling potential exists as long as the rf cavity is located in a dispersive region. However, the transverse cooling rates are low if the working point is far away from the resonance. We can further enhance the transverse cooling efficiency in the off-resonant region by switching on a coupling cavity. The dotted curves in Fig. 6 correspond to the cases where the coupling cavity has been excited with different rf powers. We clearly see the remarkable improvement of final emittances. Concerning the electrode voltage, V_c of less than a few hundred V seems to suffice for achieving transverse temperatures comparable to
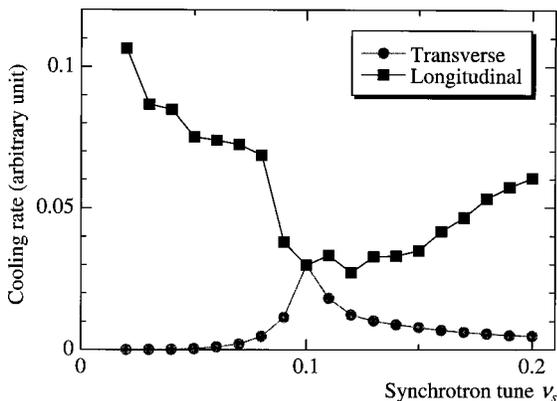
FIG. 7. Approximate cooling rates evaluated from SAD simulations, where no coupling cavity has been activated. The simple linear friction model has been used. The horizontal and vertical cooling rates are identical.
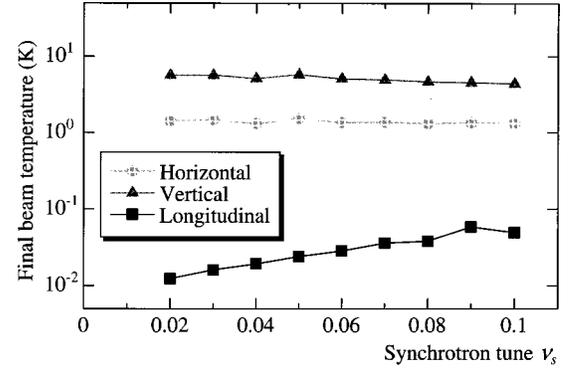
FIG. 8. Equilibrium beam temperature vs operating synchrotron tune, obtained from SOLID. The same resonant ASTRID lattice as employed in Fig. 6 has been considered, namely, $\nu_x = 3.11$, $\nu_y = 3.09$, $\Gamma_q = 0.48$, and $h_b = 260$. The coupling cavity has been switched off. The cooling strength parameter is $\lambda_s = 0.9$. The minimum transverse temperature reached with the coupling method is certainly much lower than that experimentally achieved in ASTRID. Notice also that there still exists significant temperature imbalance between the longitudinal and transverse degrees of freedom.

the longitudinal final value. Note here that the value of V_c does not represent the actual potential "felt" by stored ions. For instance, when $V_c = 500$ V, the maximum linear coupling potential at the horizontal position $x = 1$ cm is only 14.37 V according to Table I. As the transverse dimension of a cooled beam is typically even much smaller than 1 cm, the coupling-cavity parameters considered in Fig. 6 is indeed practical to implement.

V. MOLECULAR DYNAMICS RESULTS

We are now ready to examine the effect of space charges on the cooling efficiency, employing the MD code SOLID [18]. In this code, we numerically iterate the equations of motion, incorporating the characteristics of actual storage rings like bending and straight sections, and alternating gradient focusing, as we did in the SAD simulations. A Ewald-type [19] summation is performed in the azimuthal direction to evaluate the long-ranged Coulomb forces among particles, and their image charges modeled in periodic "supercells" for computing efficiency. In the following MD simulations, we always set the initial beam temperatures to be a few hundred kelvins in all three directions since this range of tem-

TABLE III. The main TARN II parameters.

Quantity	Value
Ring circumference $2\pi R$	77.7 m
Betatron tunes (ν_x, ν_y)	(2.096, 2.104)
Dipole bending radius	4.01 m
Skew quadrupole strength	0.001 m^{-1}
Lattice superperiodicity N_l	6
Transition energy γ_T	2.258
Ion species	^{24}Mg$^+$
Kinetic energy	1 MeV
rf harmonic number $(h_b = h_c)$	1000

perature can be accomplished, e.g., with the electron cooling technique. Furthermore, for the sake of reducing the computing time, a simplified cooling model is adopted; that is, we use the linear transformation

$$\left(\frac{\delta p}{p}\right)_{\text{out}} - \left(\frac{\delta p}{p}\right)_{\text{in}} = \lambda_s \left(\frac{\delta p}{p}\right)_{\text{in}}, \qquad (13)$$

where $(\delta p/p)_{\text{in}}$ and $(\delta p/p)_{\text{out}}$ are the momentum deviation before and after the cooling section, and λ_s is proportional to the cooling strength. While the model is rather crude, no fundamental difference from SAD results has so far been identified in the high temperature regime.

The first example is the resonant ASTRID lattice studied in Sec. IV. Figure 8 illustrates the ν_s dependence of the final beam temperature where the total number of stored $^{24}\text{Mg}^+$ ions is 2.6×10^4. It is shown that the present coupling method achieved transverse temperatures of the order of 1 K. Of particular interest is that the achievable lowest temperature is almost independent of the synchrotron tune in this ultracold regime, where the Coulomb coupling is effective. At high temperature, however, the transverse cooling process is extremely slow unless the synchrotron tune is near the resonant value. In fact, in order to save computing time when $\nu_s < 0.05$, we must initially employ a rf voltage close to the optimum resonant value until the beam becomes sufficiently cold. (The voltage is adjusted to a proper value after the transverse temperature has reached around a few tens of kelvins.) In all these cases, beam crystallization cannot be realized.
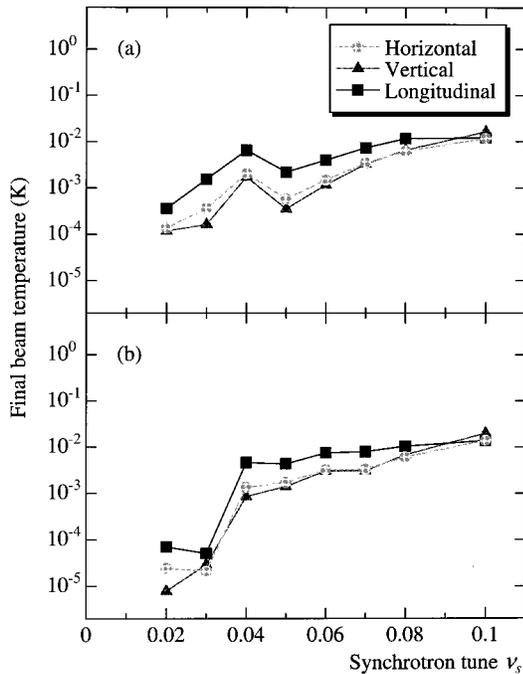
FIG. 9. Equilibrium beam temperature vs operating synchrotron tune, obtained from SOLID. The TARN II parameters listed in Table III have been employed. The upper and lower figures show the equilibrium temperatures achieved by the dispersive coupling scheme and by the coupling-cavity scheme respectively. Here, λ_s has been set at 0.9, and the total stored ions are 10^5.
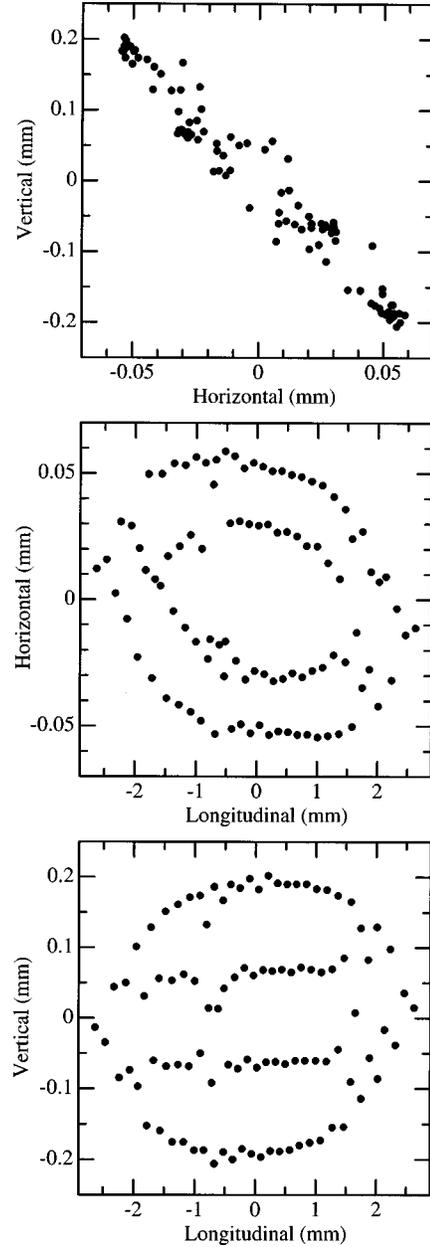
FIG. 10. Real-space profiles of a 1-MeV $^{24}\text{Mg}^+$ beam laser cooled with the dispersive-coupling scheme in the TARN II ring.

As is well-known, the lattice of a storage ring suitable for beam crystallization must fulfill the so-called *maintenance condition* given by [20]

$$\max(\nu_x, \nu_y) < \frac{N_l}{2\sqrt{2}}, \qquad (14)$$

where N_l is the lattice superperiodicity. Since neither ASTRID nor TSR meet this requirement, we here take, among a wide range of choice, the lattice parameters of TARN II [21] to investigate the role of the maintenance condition. The TARN II ring, with a circumference of 77.7 m, has a design of sixfold symmetry. Each lattice period contains four bending magnets with an orbit curvature of 4.01 m. For vertical-horizontal coupling, we put a skew quadrupole magnet in every period, keeping the high superperiod-

icity. The coupling constant defined by Eq. (3) is 0.0124. Other main parameters used in the present TARN II simulations are summarized in Table III. In order for the betatron tunes to satisfy Eq. (14) and the resonance condition simultaneously, we choose the gradients of the focusing quadrupole fields such that $(\nu_x,\nu_y)=(2.096,2.104)$. Then, according to Eq. (1), the synchrobetatron coupling is most effective when $\nu_s\approx0.1$.

The beam temperatures achieved in TARN II by means of the coupling method are plotted in Fig. 9. We see that the transverse temperatures have now become more than two orders of magnitude lower than those in the ASTRID case. Moreover, the strange temperature anisotropy observed in ASTRID has disappeared. The beam temperatures reached in these numerical experiments are already beyond the border of phase transition to an ordered state. Figure 10 displays the real-space profile of the $^{24}Mg^+$ beam in an equilibrium state in TARN II. As anticipated, a 3D ordered structure has been formed.

Figure 9 also indicates that, similar to the ASTRID case in Fig. 8, a higher transverse cooling rate does not always yield a lower beam temperature. The equilibrium temperature tends to be even lower at a smaller synchrotron tune, regardless of the fact that the transverse cooling efficiency certainly is low in the off-resonant region. Furthermore, the coupling cavity does not improve the final temperature, although it significantly shortens the cooling time. These results strongly suggest that transverse cooling rate itself may not be of essential importance *for cold beams*, at least from the viewpoint of the achievable temperature.

In order to confirm this result, we explore the cooling efficiency as functions of the cooling power. We obtained the λ_s dependence of the minimum beam temperature as illustrated in Fig. 11, showing a sudden jump around $\lambda_s \approx0.3$ [22]. Once λ_s exceeds the threshold value, the equilibrium temperature stays at an almost constant level. This observation supports the above expectation that the lowest temperature achievable in a particular direction is independent of the cooling rate in that direction as long as the beam is cold. The issue is how much *total* cooling power one can apply to a stored beam. Finally, for reference, in Fig. 12 we show the equilibrium temperatures obtained with different number of stored ions. No noticeable dependence of temperature has been found on the total number of ions in the storage ring.

VI. DISCUSSION

In spite of the past experimental observations in TSR and ASTRID, the MD results given in Sec. V naturally lead us to the conclusion that longitudinal laser cooling of fast stored beams can be equally efficient in all three degrees of freedom [23]. If so, what has caused such a large imbalance between longitudinal and transverse temperatures in these storage rings? The answer is just behind Eq. (14). The mean property of a cold circulating beam can be approximately described by the envelope equations familiar in the standard theory for linear transport systems. It is then straightforward to show that the envelope motion can be unstable due to the Mathieu resonance [24]. Equation (14) is actually nothing but the condition for extremely space-charge-dominated beams to avoid half-integer Mathieu stopbands [24,25]. Recalling that
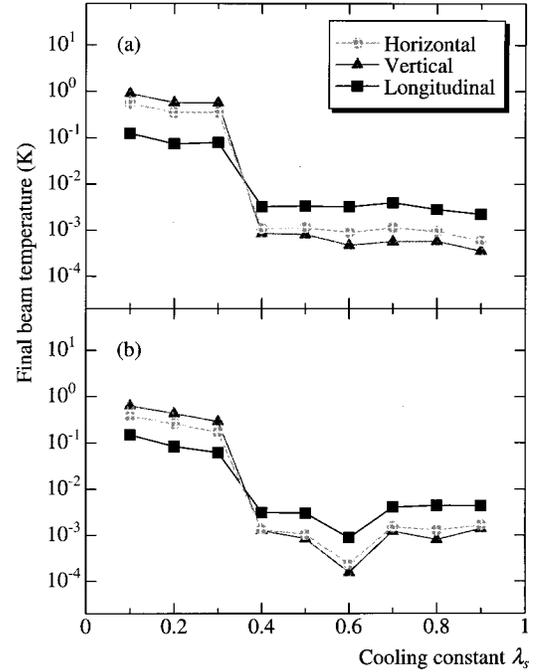
FIG. 11. Dependence of equilibrium beam temperature on longitudinal cooling power. The synchrotron tune has been fixed at 0.05, and the total number of stored ions is 10^5. In the upper picture, only the dispersive coupling in the regular rf cavity has been considered, while, in the lower picture, the coupling cavity has been excited simultaneously.

the maintenance condition has been broken in both TSR and ASTRID, high-density ion beams laser cooled in these machines are always inside a Mathieu stopband and, therefore, simply unstable in the transverse directions. Consequently,
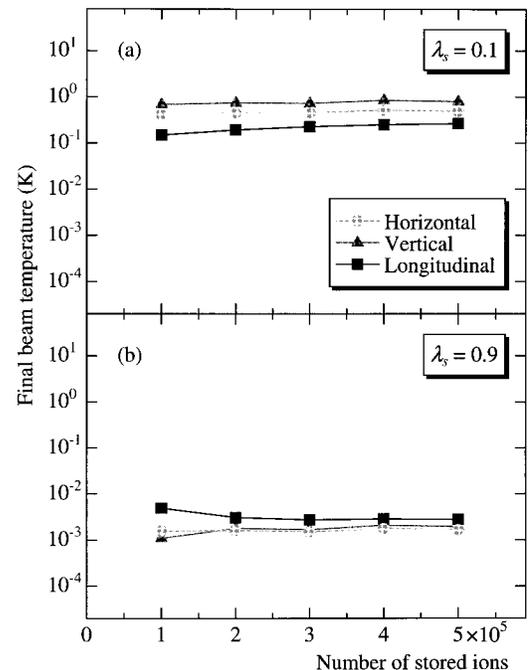
FIG. 12. Equilibrium beam temperature vs total number of stored ions at $\lambda_s=0.1$ (upper) and 0.9 (lower). The TARN II parameters given in Table III have again been assumed.
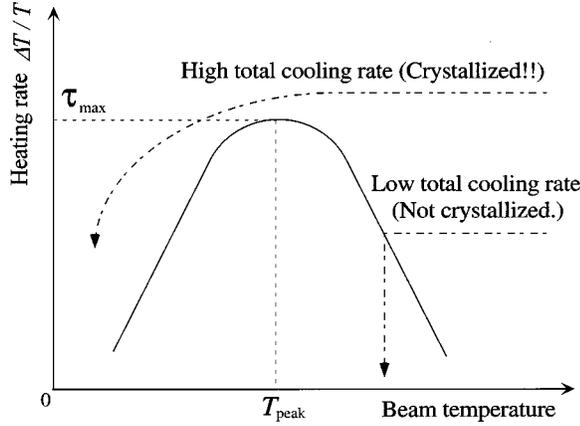
FIG. 13. Schematic drawing of a typical heating-rate curve. The heating rate $\tau = \Delta T/T$ is the rate of temperature increase in the absence of cooling force, which can be evaluated from MD calculation.

the transverse equilibrium temperatures can never be reduced to the TARN II level [26,27]. During the present MD study, we have also recognized that, unlike the TARN II case, the time evolution of beam temperature in ASTRID is often quite spiky since captured ions tend to escape from the rf buckets. The primary source of this spiky behavior can again be attributed to the Mathieu instability rather than to binary Coulomb collisions. Hence the temperature anisotropy experimentally detected in TSR and ASTRID should not be interpreted as evidence that transverse motion of fast stored beams can only be cooled weakly by longitudinal laser light.

In principle, a storage-ring system for low-energy ions is similar to a rf quadrupole (RFQ) ion-trap system, except for the existence of momentum dispersion induced by bending magnets. (The contribution of dipole fields is almost separable in the stationary state of space-charge-dominated beams [24].) Accordingly, what happened in a rf trap can also happen in a storage ring. Since a single laser in the longitudinal direction is adequate to make a crystal in a RFQ ion trap, this longitudinal cooling force should also sympathetically produce a strong transverse friction in fast stored beams at low temperature. On the other hand, stored ions feel a rf force in the beam frame as they are circulating around the system at great speed. In order to gain insight into the beam stability behavior, it is suggestive that the stability of crystals in rf traps can be studied under controlled Mathieu-type instability conditions [28].

The dispersive effect peculiar to storage-ring systems imposes a special demand upon the nature of cooling force for stabilizing crystals. Since the revolution frequencies of all ions forming a crystalline beam are identical in order to maintain its ground-state structure, a longitudinal laser must provide such a cooling force as to give a greater average velocity to a radially outer particle. This is referred to as *tapered cooling* [20,29]. If too powerful an *untapered* laser is applied, multidimensional crystalline structures can be easily destroyed, since the laser simply equalizes the longitudinal velocities of all particles.

We now give a plausible explanation as to why there is a jump of equilibrium temperature in Fig. 11. The heating-rate diagram shown in Fig. 13 provides insight in this regard.

Interestingly, the basic feature of the diagram is insensitive to the lattice design, stored ion species, beam energy, etc., according to the past MD studies [30], as long as the crystalline-beam maintenance condition is satisfied. For an ideal storage ring free from field imperfections, the peak heating rate τ_{max} due to random Coulomb collisions has been found to be typically of the order of 0.1. To attain a crystalline beam, we must overcome this peak. If the available cooling rate is less than the maximum heating rate, we will inevitably hit the high-temperature side of the heating-rate mountain in Fig. 13 and fail to go beyond the peak to beam crystallization. On the other hand, once the cooling rate exceeds the peak heating rate, we can reach the crystalline state. This is the reason why the sudden change of equilibrium temperature occurs at a specific value of λ_s. The minimum cooling power required for beam crystallization is the product of beam temperature and the corresponding heating rate. This product usually becomes maximum at around $T \approx T_{peak}$. The energy removed by a single traversal of cooling section should thus be greater than, at least, $\tau_{max}T_{peak}$ (in kelvins). Since T_{peak} is $1-10$ K and $\tau_{max} \approx 0.1$ in most cases, the cooling power of $0.1-1$ K/turn will be necessary for our final goal.

Finally, we again emphasize the practical importance of the resonant coupling method explored in this paper. Since the method does not rely on mutual particle interactions, one can readily bring any high-temperature beam to an ultracold state within a very short cooling time, independent of the ion density. In contrast, in the case of sympathetic cooling the stored beam must be initially dense enough to develop strong Coulomb coupling; otherwise, the cooling time may become unreasonably long or it may be simply impossible to cool betatron motions. In practice, we will need artificial coupling to quickly reduce the transverse temperature of initial hot beams. As demonstrated in the present MD simulations, it is possible to realize a Coulomb ordering, by means of the resonant coupling method, if the storage-ring lattice is properly designed [31].

APPENDIX

When $\nu_s \ll 1$, one can approximately rewrite Eq. (2) by smoothing the synchrotron motion, as

$$\tilde{H}_1 = \frac{\nu_x}{2}(\tilde{p}_x{}^2 + \tilde{x}^2) + \frac{\nu_s}{2}(\tilde{p}_z{}^2 + \tilde{z}^2) - \xi\tilde{z}\tilde{p}_x\delta_p(\theta - \theta_b)$$

where the vertical motion as well as the higher-order terms has been neglected for brevity, the θ derivative of D_x has been assumed to be zero at the cavity location, and the new canonical variables are given by

$$(\widetilde{x},\widetilde{p}_x,\widetilde{z},\widetilde{p}_z)=\left(\sqrt{\nu_x}x, \frac{p_x}{\sqrt{\nu_x}}, \sqrt{\frac{h_b q V_b}{2\pi\nu_s p_0 \beta_0 c}}\psi, \sqrt{\frac{|\eta|}{\nu_s}}W \right) .$$

The parameter ξ, which determines the strength of synchrobetatron coupling, is defined by Eq. (8). The one-turn transfer matrix **M** for this coupled motion can be diagonalized to a 2×2 form as

$$\mathbf{U M U}^{-1}=\begin{pmatrix} \mathbf{M_1} & \mathbf{0} \\ \mathbf{0} & \mathbf{M_2} \end{pmatrix},$$

with

$$\mathbf{U}=\begin{pmatrix}
\alpha & 0 & -\kappa[\cos(2\pi\nu_x)-\cos(2\pi\nu_s)] & -\kappa\sin(2\pi\nu_s) \\
0 & \alpha & \kappa\sin(2\pi\nu_x) & 0 \\
0 & -\kappa\sin(2\pi\nu_s) & \alpha & 0 \\
\kappa\sin(2\pi\nu_x) & \kappa[\cos(2\pi\nu_x)-\cos(2\pi\nu_s)] & 0 & \alpha
\end{pmatrix},$$

where, by using the parameter g in Eq. (7), we have

$$\alpha=\sqrt{\frac{1+g}{2}} \quad\text{and}\quad \kappa^2\sin(2\pi\nu_x)\sin(2\pi\nu_s)=\frac{1-g}{2} .$$

Assuming a uniform longitudinal damping along the ring circumference, the cooling rates are given by the diagonal parts of the matrix $\mathbf{U V U}^{-1}$, where

$$\mathbf{V}=\begin{pmatrix}
\cos(2\pi\nu_x) & \sin(2\pi\nu_x) & 0 & 0 \\
-\sin(2\pi\nu_x) & \cos(2\pi\nu_x) & 0 & 0 \\
0 & 0 & e^{-\Lambda}\cos(2\pi\nu_s) & e^{-\Lambda}\sin(2\pi\nu_s) \\
0 & 0 & -e^{-\Lambda}\sin(2\pi\nu_s) & e^{-\Lambda}\cos(2\pi\nu_s)
\end{pmatrix}\begin{pmatrix}
1 & 0 & -\xi & 0 \\
0 & 1 & 0 & 0 \\
0 & 0 & 1 & 0 \\
0 & \xi & 0 & 1
\end{pmatrix}-\mathbf{M}$$

$$\approx-\Lambda\begin{pmatrix}
0 & 0 & 0 & 0 \\
0 & 0 & 0 & 0 \\
0 & 0 & \cos(2\pi\nu_s) & \sin(2\pi\nu_s) \\
0 & 0 & -\sin(2\pi\nu_s) & \cos(2\pi\nu_s)
\end{pmatrix}\begin{pmatrix}
1 & 0 & -\xi & 0 \\
0 & 1 & 0 & 0 \\
0 & 0 & 1 & 0 \\
0 & \xi & 0 & 1
\end{pmatrix}.$$

After some straightforward algebra, we obtain the cooling-rate formulas in Eqs. (6).

[1] S. van der Meer, CERN Report No. CERN/TSR-PO/72-31 (1972).

[2] G. I. Budker, At. Energ. **22**, 345 (1967).

[3] D. J. Wineland and H. Dehmelt, Bull. Am. Phys. Soc. **20**, 637 (1975); T. Hänsch and A. Schawlow, Opt. Commun. **13**, 68 (1975).

[4] A. Rahman and J. P. Schiffer, Phys. Rev. Lett. **57**, 1133 (1986); R. W. Hasse and J. P. Schiffer, Ann. Phys. (N.Y.) **203**, 419 (1990); J. P. Schiffer, Phys. Rev. Lett. **70**, 818 (1993); J. Wei, X-P. Li, and A. M. Sessler, Brookhaven National Laboratory Report No. BNL-52381 (1993); Phys. Rev. Lett. **73**, 3089 (1994).

[5] S. Schröder, R. Klein, N. Boos, M. Gerhard, R. Grieser, G. Huber, A. Karafillidis, M. Kieg, N. Schmidt, T. Kühl, R. Neumann, V. Balykin, M. Grieser, D. Habs, E. Jaeschke, D. Krämer, M. Kristensen, M. Music, W. Petrich, D. Schwalm, P. Sigray, M. Steck, B. Wanner, and A. Wolf, Phys. Rev. Lett. **64**, 2901 (1990).

[6] J. S. Hangst, M. Kristensen, J. S. Nielsen, O. Poulsen, J. P. Schiffer, and P. Shi, Phys. Rev. Lett. **67**, 1238 (1991).

[7] H-J. Miesner, R. Grimm, M. Grieser, D. Habs, D. Schwalm, B. Wanner, and A. Wolf, Phys. Rev. Lett. **77**, 623 (1996).

[8] H. Okamoto, A. M. Sessler, and D. Möhl, Phys. Rev. Lett. **72**, 3977 (1994).

[9] H. Okamoto, Phys. Rev. E **50**, 4982 (1994).

[10] I. Lauer, U. Eisenbarth, M. Grieser, R. Grimm, P. Lenisa, V. Luger, T. Schätz, U. Schramm, D. Schwalm, and M. Weidemüller, Phys. Rev. Lett. **81**, 2052 (1998). In the laser-cooling experiment reported in Ref. [10], a transverse linear coupling resonance ($\nu_x-\nu_y\approx0$) was actually employed to improve the vertical cooling efficiency. As clearly seen in Fig. 3 in this reference paper, the vertical cooling rate becomes equal to the horizontal rate with the resonance condition satisfied. This experimental observation indicates that the idea of indirect resonant cooling studied in Refs. [8] and [9] is basically correct. Since there is no substantial difference between the horizontal-vertical and longitudinal-horizontal coupling, as is shown in Ref. [9], the transverse dissipative force can be enhanced only by driving the ring operating point onto a synchrobetatron resonance. (In both TSR and ASTRID, a rf cavity

is already located at a dispersive position. Thus, a linear synchrobetatron coupling potential required for our resonant coupling scheme in Sec. II A is always available in bunched-beam laser cooling.)

[11] For the details of the SAD code, see http://www-acc-theory.kek.jp/SAD/sad.html

[12] The three sets of the canonical variables, (x,p_x), (y,p_y), and (ψ,W), describe the horizontal, vertical, and longitudinal motion, respectively. The detailed derivation of Eq. (2) is available in Ref. [9].

[13] H. Okamoto, S. Machida, and A. M. Sessler, in *Crystalline Beams and Related Issues*, edited by D. M. Maletic and A. G. Ruggiero (World Scientific, Singapore, 1996), p. 173.

[14] To excite a synchrobetatron coupling resonance, the longitudinal tune must be nonzero.

[15] There may be a solution utilizing the nonlinear coupling in order to raise the transverse cooling efficiency. In such a case, one may choose h_c greater than h_b to increase the strength of the nonlinear contributions. This is a future issue to study.

[16] J. S. Hangst, J. S. Nielsen, O. Poulsen, P. Shi, and J. P. Schiffer, Phys. Rev. Lett. **74**, 4432 (1995). Theoretically speaking, one can apply much higher voltage with no problem. However, in practice, the application of too high a voltage is dangerous, since it may heat up the cold beams, e.g., due to the inevitable noises of the rf system. It is thus better to use as low a rf voltage as possible.

[17] See, e.g., *User's Guide for the POISSON/SUPERFISH Group of Codes*, LA-UR-87-115 (Los Alamos National Laboratory, Los Alamos, 1987).

[18] For the information about SOLID, see, e.g., J. Wei, X.-P. Li, and A. M. Sessler, BNL-52387 (1993).

[19] P. P. Ewald, Ann. Phys. (Leipzig) **64**, 253 (1921).

[20] See, e.g., J. Wei, A. Draeseke, A. M. Sessler, and X.-P. Li, in *Crystalline Beams and Related Issues* (Ref. [13]), p. 229.

[21] T. Katayama, A. Andou, K. Chida, T. Hattori, T. Honnma, K. Kanazawa, A. Mizobuchi, H. Mutou, N. Nakai, S. Ninomiya, A. Noda, K. Noda, M. Sekiguchi, F. Soga, T. Tanabe, N. Ueda, S. Watanabe, T. Watanabe, and M. Yoshizawa, in *Proceedings of the 2nd European Particle Accelerator Conference*, edited by P. Martin and P. Mandrillon (Editions Frontières, Gif-sur-Yvette, 1990), p. 577.

[22] The value of λ_s at which the temperature jump takes place is roughly independent of the nature of the cooling force. For example, even in the tapered cooling scheme [29], the achievable beam temperature suddenly changes at $\lambda_s \approx 0.3$.

[23] Note, however, that the beam density must be high enough in order for the longitudinal cooling force to be sympathetically effective in transverse directions. The sympathetic transverse cooling is thus generally inefficient for common beams in storage rings. By contrast, the coupling method studied here works even for low-density initial beams, since it has nothing to do with the Coulomb interactions.

[24] S. Y. Lee and H. Okamoto, Phys. Rev. Lett. **80**, 5133 (1998).

[25] The maintenance condition is, therefore, not limited to crystalline beams. At the high-temperature limit, Eq. (14) is changed to $\max(\nu_x,\nu_y) < N_l/4$ [or, equivalently, $\max(\mu_x,\mu_y) < \pi/2$ where μ_x and μ_y denote, respectively, horizontal and vertical betatron phase advances per lattice period. This condition is identical to the well-known design criterion for high-intensity linear transport systems.]

[26] T. Kihara, H. Okamoto, Y. Iwashita, K. Oide, G. Lamanna, and J. Wei, in *Proceedings of the 6th European Particle Accelerator Conference*, edited by S. Myers, L. Liljeby, Ch. Petit-Jean-Genaz, J. Poole, and K.-G. Rensfelt (Institute of Physics Publishing, Bristol, 1998), p. 1040.

[27] N. Madsen, P. Bowe, M. Drewsen, L. Hornekaer, N. Kjaergaard, A. Labrador, P. Shi, J. S. Hangst, J. S. Nielsen, and J. P. Schiffer, in *Proceedings of the 6th European Particle Accelerator Conference* (Ref. [26]), pp. 1043 and 1046; In this reference, researchers from Aarhus University have reported on an interesting experimental observation which suggests that the transverse beam quality in the ASTRID ring may be limited by some resonance mechanism. Although further investigation is necessary, we speculate that the result may be explained by the Mathieu instability discussed here.

[28] It has been experimentally verified that ions confined in a rf trap system are immediately lost unless the design parameters of the system, such as the rf voltage, the operating frequency, etc., are properly chosen to avoid the Mathieu instability.

[29] J. Wei, H. Okamoto, and A. M. Sessler, Phys. Rev. Lett. **80**, 2606 (1998); H. Okamoto and J. Wei, Phys. Rev. E **58**, 3817 (1998); J. P. Schiffer, in *Crystalline Beams and Related Issues* (Ref. [13]), p. 217.

[30] See, e.g., J. Wei, A. Draeske, A.M. Sessler, and Xi Pi Li, in *Crystalline Beams and Related Issues* (Ref. [20]), Fig. 3; J.P. Schiffer, in *ibid.*, Fig. 2.

[31] Since the 1D string structure has no transverse extent, it is free from the Mathieu instability. It may thus be possible to create string crystals even in ASTRID and TSR. However, considering that sympathetic cooling is extremely slow, or simply negligible for such a low-density beam, the resonant coupling method must be applied.